Int. J. Adv. Res. Sci. Technol. Volume 15, Issue 10, 2026, pp. 163-172.

IJARST

International Journal of Advanced Research in Science and Technology

https://doi.org/10.62226/ijarst20262858

ISSN 2319 – 1783 (Print)

ISSN 2320 – 1126 (Online)

Three-Dimensional Hydrostatic and Biaxial Strain Distributions in a Pyramidal InAs/GaAs Quantum Dot: An Aspect-Ratio-Based Computational Analysis

Hasan Hamada Ali

Department of Physics, College of Education for Pure Sciences, Tikrit University Salahaddin, 44001, Iraq

hassan.h.ali@tu.edu.iq, https://orcid.org/0009-0000-9718-4907

ARTICLEINFO

Article history:

Received	13 Oct 2026
Accepted	20 Oct 2026
Available online	28 Oct 2026

Keywords:

Hydrostatic strain, biaxial strain, lattice mismatch, aspect ratio, three-dimensional strain distribution, strain reconstruction, InAs/GaAs quantum dot, pyramidal quantum dot, and semiconductor nanostructures.

Indexed in:

and in major libraries

ABSTRACT

Strain induced by lattice mismatch is a fundamental characteristic of self-assembled InAs/GaAs quantum dots and plays an important role in determining their local mechanical state and, consequently, their potential electronic and optoelectronic behavior. In this work, an aspect-ratio-dependent computational strain library built inside a MATLAB-based reconstruction framework is used to examine the three-dimensional distributions of hydrostatic and biaxial strain in a square-based pyramidal InAs/GaAs quantum dot. The computational method uses geometric symmetry expansion and three-dimensional spatial interpolation to obtain the strain distribution over the specified computational domain by reconstructing the spatial strain field from precomputed strain data corresponding to chosen quantum-dot aspect ratios. The normal components of the strain tensor are used to derive the hydrostatic and biaxial strain components, which offer complementary explanations of the local deformation. The biaxial strain is defined as $\varepsilon_B=\varepsilon_{xx}+\varepsilon_{yy}-2\varepsilon_{zz}$, which represents the directional difference between the in-plane and growth-direction deformation, while the hydrostatic strain is defined as $\varepsilon_H=\varepsilon_{xx}+\varepsilon_{yy}+\varepsilon_{zz}$, which represents the volumetric component of deformation. The analysis takes into consideration the significant lattice mismatch between InAs and GaAs and investigates the spatial properties of the reconstructed strain fields with respect to the aspect ratio and pyramidal quantum-dot geometry. A highly non-uniform strain distribution is revealed by the reconstructed three-dimensional data, especially in the quantum-dot region and close to the InAs/GaAs heterointerface. Within the InAs quantum dot, the hydrostatic strain responds primarily in a compressive manner before gradually relaxing spatially toward the surrounding GaAs matrix. The anisotropic nature of the local deformation and the distinction between the in-plane and growth-direction strain components are reflected in the biaxial strain's more varied distribution. The minimum and maximum strain values, along with the accompanying spatial coordinates, centerline profiles, cross-sectional distributions, interface behavior, and spatial relaxation, are used for quantitative characterization. Beyond the qualitative interpretation of color maps, these characteristics offer a repeatable foundation for assessing the reconstructed strain field. The findings show that the amount and spatial localization of the reconstructed hydrostatic and biaxial strain components are influenced by lattice mismatch, quantum-dot geometry, and aspect ratio. The resulting three-dimensional strain fields can be used as input for later deformation-potential, multiband k·p, or atomistic electronic-structure computations, and they offer a quantitative mechanical description of the pyramidal InAs/GaAs quantum-dot system. Crucially, the current study does not explicitly compute electronic band structures, carrier wave functions, optical transition energies, emission spectra, carrier transport, or device performance; instead, it is limited to mechanical strain reconstruction. Therefore, conclusions concerning these properties require an additional electronic-structure model.

© 2026 The Authors. This work is licensed under a Creative Commons Attribution 4.0 License. For more information, see https://creativecommons.org/licenses/by/4.0/

1. Introduction

Because of their three-dimensional carrier confinement, which produces discrete electronic states and permits the tailoring of optical transition energies, self-assembled semiconductor quantum dots (QDs) are significant nanoscale structures for optoelectronic applications [1-4]. Due to its significant lattice mismatch and importance for quantum-dot lasers, photodetectors, and other optoelectronic devices, InAs/GaAs quantum dots have drawn a lot of attention among the III-V semiconductor systems [5]. When InAs islands are coherently generated within or on a GaAs matrix, there is a significant lattice mismatch since the bulk lattice constants of InAs and GaAs are roughly 6.0583"Å" and 5.6533"Å," respectively. The quantum dot and the surrounding semiconductor material experience elastic deformation as a result of this mismatch [6–9].

The resulting strain field is inherently non-uniform and is not confined to the volume of the quantum dot. Rather, the

elastic deformation is spatially dependent on the boundary conditions, quantum-dot shape, and material mismatch and extends into the surrounding GaAs matrix [10,11]. A reliable description of this strain field is therefore essential for characterizing the mechanical state of the heterostructure and for providing appropriate input to subsequent calculations of strain-dependent electronic properties. In particular, hydrostatic and biaxial strain are useful quantities for describing complementary aspects of the strain tensor in zinc-blende semiconductor quantum dots. The hydrostatic component represents the volumetric deformation, whereas the biaxial component describes the directional difference between the in-plane and growth-direction deformation [12,13].

Strain in silicon quantum dots has been described using a variety of theoretical and computational methods. Continuum elasticity has been used to quantum dots with various geometries and offers an effective framework for getting analytical or semi-analytical answers. For instance, formulations based on Green's function have been created for quantum dots of any shape, taking into consideration the impact of elastic anisotropy [13,14]. Additionally, analytical treatments for buried pyramidal quantum dots have been proposed, showing that the quantum-dot shape and the assumptions made for the elastic media have a significant impact on the strain's amplitude and spatial distribution.

These approaches provide valuable physical insight while offering relatively efficient descriptions of strain distributions[15,16].

Atomistic methods provide a complementary approach by explicitly describing the relaxation of individual atomic positions. Such methods are particularly relevant for highly strained semiconductor heterostructures, where local structural effects near interfaces, edges, and vertices may be important. Previous atomistic investigations have demonstrated that the strain distribution in InAs/GaAs quantum dots depends strongly on the quantum-dot aspect ratio and geometry[17,18]. The universal-strain framework introduced in previous work further demonstrated that aspect-ratio-dependent atomistic strain distributions can be represented using compact strain descriptions, thereby providing a practical connection between detailed atomistic calculations and computational strain reconstruction[19].

Despite these developments, an important distinction must be maintained between strain generation and strain-field reconstruction. A computational framework based on precomputed strain data does not constitute an independent elasticity or atomistic relaxation solver. Instead, its reliability depends on how the underlying strain data are represented, selected, transformed, and interpolated [20,21]. Consequently, a reproducible reconstruction procedure should explicitly define the material system, quantum-dot geometry, aspect-ratio dependence, coordinate system, spatial normalization, symmetry operations, interpolation procedure, and physical definitions of the reconstructed strain quantities. Without such information, three-dimensional strain maps may be difficult to reproduce or to interpret quantitatively [22].

Previous studies have established analytical, continuum, and atomistic methodologies for calculating strain distributions in semiconductor quantum dots. However, the systematic reconstruction and quantitative interpretation of available three-dimensional hydrostatic and biaxial strain fields for a pyramidal InAs/GaAs quantum dot remain important from a computational and methodological perspective [23,24]. In particular, there is a need to move beyond qualitative descriptions based solely on color maps and instead characterize the reconstructed fields using numerical extrema, their spatial locations, centerline profiles, interface behavior, and spatial relaxation [25,26]. The present study addresses this computational problem using an aspect-ratio-dependent strain representation for a square-based pyramidal InAs/GaAs quantum dot. The supplied MATLAB framework employs a precomputed strain library containing hydrostatic and biaxial strain data for selected aspect ratios. When the requested aspect ratio corresponds to a library entry, the associated strain field is directly selected. For an intermediate aspect ratio, the neighboring library solutions are interpolated with respect to aspect ratio. The reconstructed field is subsequently expanded according to the geometric symmetry of the pyramidal structure and interpolated spatially to obtain the three-dimensional strain distribution within a common computational coordinate system [27-29].

The main objective of this work is therefore not to introduce a new fundamental elasticity solution, but to establish a systematic and quantitatively interpretable procedure for reconstructing and analyzing the available three-dimensional hydrostatic and biaxial strain fields. Particular attention is given to the minimum and maximum strain values, their spatial coordinates, centerline profiles, behavior across the InAs/GaAs interface, spatial relaxation into the surrounding GaAs matrix, and the influence of the quantum-dot aspect ratio. Compared to qualitative examination of three-dimensional color maps alone, this method offers a more consistent interpretation of the mechanical strain field. For later deformation-potential, multiband k·p, or atomistic electronic-structure computations, the reconstructed strain fields are meant to offer a physically consistent mechanical input. Crucially, electronic band structures, carrier wave functions, optical transition energies, carrier transport, and device performance are not directly calculated in this study. As a result, the estimated strain fields provide the mechanical foundation needed for such further analyzes, rather than quantitatively inferring electrical and optical effects from the strain distributions alone. As a result, the main contributions of this work are:

Three-dimensional strain reconstruction: reconstruction of hydrostatic and biaxial strain fields for a square-based pyramidal InAs/GaAs quantum dot using an aspect-ratio-dependent precomputed strain library.

1. Consistent strain characterization: explicit definition and separation of the hydrostatic and biaxial strain components and their adopted sign conventions.
2. Quantitative spatial analysis: determination of strain extrema, their corresponding spatial coordinates, centerline profiles, interface behavior, and spatial relaxation within the quantum-dot/matrix system.

3. Geometrical and aspect-ratio analysis: systemati- examination of the influence of quantum-dot geometry and aspect ratio on the magnitude an ↓atial localization of the reconstructed strain components.
4. Basis for subsequent electronic analysis: establishment of a quantitatively characterized mechanical strain field that can be used as input for subsequent deformation-potential or multiband electronic-structure calculations.

2. Theory

The strain state of the InAs/GaAs heterostructure is described by the symmetric strain tensor[30].

$$\varepsilon - \begin{bmatrix} \varepsilon_{xz} & \varepsilon_{xy} & \varepsilon_{xz} \\ \varepsilon_{xy} & \varepsilon_{yy} & \varepsilon_{yz} \\ \varepsilon_{xz} & \varepsilon_{yz} & \varepsilon_{zz} \end{bmatrix} \dots (1)$$

Figure 1 illustrates how the stress is concentrated at the dot's center, how it progressively diminishes toward the edges or substrate, and how material differences and crystal boundaries cause it to vary vertically as opposed to horizontally[31,32].

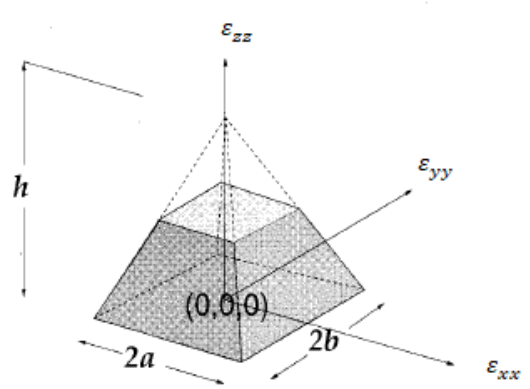


Figure 1: Geometrical parameters defining a pyramidal quantum dot in the center of the quantum dot in the fundamental plane, is the coordinate system's origin [33].

The InAs/GaAs system exhibits a substantial lattice mismatch because the equilibrium lattice constant of InAs is larger than that of GaAs. The lattice-mismatch parameter is defined as [34]:

$$\varepsilon_0 = \frac{a_{\ln \Lambda s} - a_{GiaAs}}{a_{\ln \Lambda s}} \dots (2)$$

where a_{InAs} and $a_{\mathrm{Ga.As}}$ denote the unstrained bulk lattice constants of InAs and GaAs, respectively. Using

$$a_{\mathrm{In}\lambda\,\mathrm{s}} \approx 6.0583, a_{\mathrm{GaA\,s}} \approx 5.6533,$$

gives

$$\varepsilon_0 \approx 0.06685 \approx 6.7\% \dots (3)$$

The lattice mismatch represents the initial misfit between the two materials and should not be confused with the final local strain. The local strain results from elastic relaxation and therefore varies spatially throughout the quantum-dot/matrix system[35].

The hydrostatic strain is defined as the trace of the strain tensor:

$$\varepsilon_{\mathrm{H}} - \varepsilon_{xx} + \varepsilon_{yy} + \varepsilon_{zz} \dots (4)$$

It represents the volumetric component of deformation. A negative value corresponds to local volumetric compression under the adopted sign convention, whereas a positive value corresponds to local volumetric expansion.

The hydrostatic strain is dimensionless and must not be described as pressure or stress. Hydrostatic stress is a different mechanical quantity with units of pressure and is not equivalent to hydrostatic strain.

For the [001]-oriented zinc-blende InAs/GaAs system, the biaxial strain quantity used in the present analysis is defined as

$$\varepsilon_{\mathrm{B}} - \varepsilon_{xz} + \varepsilon_{yy} - 2\varepsilon_{zz} \dots (5)$$

where x and y denote the in-plane directions and z denotes the growth direction.
The biaxial component measures the difference between in-plane and growth-direction deformation. Unlike the hydrostatic component, it does not represent a change in volume alone. It characterizes the deviatoric part of the normal strain relevant to the splitting of valence-band states in zinc-blende semiconductor models.

Strain-induced band-edge modifications are not directly calculated by the present strain-reconstruction program. Nevertheless, the calculated strain fields can be used as input to a deformation-potential model.

Under a simplified deformation-potential treatment, the conduction-band shift can be written as

$$\Delta E_{\mathrm{C}} - a_{\mathrm{C}}\varepsilon_{\mathrm{H}} \dots (6)$$

while the heavy-hole and light-hole shifts can be expressed in terms of the hydrostatic and biaxial strain components. In a commonly used convention,

$$\Delta E_{\mathrm{HH}} - a_{\mathrm{V}}\varepsilon_{\mathrm{H}} - \frac{b}{2}\varepsilon_{\mathrm{B}} \dots (7)$$

$$\Delta E_{\mathrm{LH}} - a_{\mathrm{V}}\varepsilon_{\mathrm{H}} + \frac{b}{2}\varepsilon_{\mathrm{B}} \dots (8)$$

where $a_{\mathrm{C}}, a_{\mathrm{V}}$, and b are the conduction-band hydrostatic, valence-band hydrostatic, and shear deformation potentials, respectively.

These equations are introduced to clarify the physical connection between the calculated strain field and possible electronic consequences. They are not used to claim quantitative band-edge or optical results unless the corresponding deformation-potential calculation is explicitly performed[36,37].

The supplied MATLAB implementation uses a precomputed strain library. Each library entry corresponds to a particular material system, quantum-dot shape, and aspect ratio. For the InAs/GaAs pyramidal system, the available aspect ratios are

$$AR = \frac{B}{H} \dots (9)$$

with

$$AR \in \{1,2,3,5,7,10,15,20\} \dots (10)$$

where B is the square-base length and H is the quantum-dot height.

The MATLAB implementation first calculates the aspect ratio from the user-defined base length and height. If the requested aspect ratio is directly available in the library, the corresponding data file is loaded. If the requested aspect ratio lies between two available values, the strain fields associated with the two neighboring aspect ratios are spatially interpolated and then linearly interpolated with respect to aspect ratio.

For an intermediate aspect ratio AR bounded by AR_1 and AR_2, the hydrostatic strain is reconstructed as

$$\varepsilon_{\mathrm{H}}(AR) - \frac{AR - AR_1}{AR_2 - AR_1}\varepsilon_{\mathrm{H}}(AR_1) + \frac{AR_2 - AR}{AR_2 - AR_1}\varepsilon_{\mathrm{H}}(AR_2) \dots (11)$$

and an analogous expression is used for the biaxial strain:

$$\varepsilon_{\mathrm{B}}(AR) - \frac{AR - AR_1}{AR_2 - AR_1}\varepsilon_{\mathrm{B}}(AR_1) + \frac{AR_2 - AR}{AR_2 - AR_1}\varepsilon_{\mathrm{B}}(AR_2) \dots (12)$$

The supplied implementation then expands the stored data using the geometric symmetry of the square-based pyramidal structure. Three-dimensional interpolation is subsequently performed using MATLAB's griddata procedure to reconstruct the strain field on the selected spatial grid.

The strain values stored in the library are rescaled by a factor of 10^{-4} in the MATLAB implementation. Consequently, the final reported strain values are dimensionless.

The present computational implementation uses a precomputed strain library to reconstruct the hydrostatic and biaxial strain fields of pyramidal InAs/GaAs quantum dots. Each library entry corresponds to a specified quantum-dot geometry and aspect ratio. The aspect ratio is defined as the ratio between the base length B : H and the quantum-dot height

$$AR = \frac{B}{H} \dots (13)$$

For the available pyramidal quantum-dot configurations, the strain library contains discrete aspect-ratio values. When the requested aspect ratio coincides with one of the available values, the corresponding strain field is directly selected. When the requested aspect ratio lies between two available values, the strain fields corresponding to the neighboring aspect ratios are interpolated

For an aspect ratio AR located between AR_1 and AR_2, the reconstructed hydrostatic strain is given by

$$\varepsilon_H(AR) - w_1\varepsilon_H(AR_1) + w_2\varepsilon_H(AR_2) \dots (14)$$

where the interpolation weights are

$$w_1 - \frac{AR_2 - AR}{AR_2 - AR_1} \dots (15)$$

and

$$w_2 - \frac{AR - AR_1}{AR_2 - AR_1} \dots (16)$$

with

$$w_1 + w_2 - 1 \dots (17)$$

The same interpolation procedure is applied to the biaxial strain field

$$\varepsilon_B(AR) - w_1\varepsilon_B(AR_1) + w_2\varepsilon_B(AR_2) \dots (18)$$

This procedure provides a continuous estimate of the strain field between the discrete aspect ratios represented in the precomputed library

Following aspect-ratio selection or interpolation, the stored strain data are reconstructed over the three-dimensional computational domain. The spatial coordinates are represented by:

$$\mathbf{r} - (x, y, z) \dots (19)$$

where x and y represent the in-plane directions and z represents the growth direction

The reconstructed fields can therefore be expressed as:

$$\varepsilon_H - \varepsilon_H(x, y, z) \dots (20)$$

and

$$\varepsilon_B - \varepsilon_B(x, y, z) \dots (21)$$

Three-dimensional interpolation is then applied to obtain strain values at the selected spatial coordinates. This procedure allows the discrete strain-library data to be represented as continuous three-dimensional, fields suitable for visualization and quantitative analysis. The resulting representation is subsequently used to determine the spatial extrema, centerline profiles, and interface behavior discussed in the Results section

Table 1: parameters of the InAs/GaAs system [38].

Parameter	InAs	GaAs
(a) (Å)	6.0583	5.6533
(C_{11}) (GPa)	83.29	122.1
(C_{12}) (GPa)	45.26	56.6
(C_{44}) (GPa)	39.59	60.0

To quantify the spatial variation of strain beyond the three-dimensional color maps, profiles along selected directions are extracted from the reconstructed fields. Along the central growth axis, where $x - 0$ and $y - 0$, the hydrostatic and biaxial strain profiles are expressed as

$$\varepsilon_H^c(z) - \varepsilon_H(0,0,z).. (22)$$

and

$$\varepsilon_B^c(z) - \varepsilon_B(0,0,z) \dots (23)$$

These centerline profiles provide a direct representation of how the strain changes from the substrate through the quantum-dot region and toward the upper part of the computational domain Similarly, an interface profile can be defined along a selected trajectory crossing the InAs/GaAs boundary

$$\varepsilon_i(s) - \varepsilon(\mathbf{r}(s)) \dots (24)$$

where s denotes the distance along the selected profile and $\mathbf{r}(s)$ represents its spatial coordinates

The interface profiles are particularly useful for identifying the spatial transition between the quantum-dot region and the surrounding GaAs matrix. Rather than interpreting a color transition qualitatively, the profile provides a quantitative measure of the strain variation across the interface. Because the geometry of a pyramidal quantum

dot influences the distribution of elastic deformation, the effect of aspect ratio is evaluated by comparing the reconstructed strain fields for different AR values

For a selected strain quantity ε, the variation between two aspect ratios can be expressed as

$$\Delta\varepsilon(AR_1, AR_2) - \varepsilon(AR_2) - \varepsilon(AR_1) \dots (25)$$

For the extrema, the aspect-ratio dependence can be evaluated using

$$\Delta\varepsilon_{H,\min} - \varepsilon_{H,\min}(AR_2) - \varepsilon_{H,\min}(AR_1) \dots (26)$$

and

$$\Delta\varepsilon_{B,\min} - \varepsilon_{B,\min}(AR_2) - \varepsilon_{B,\min}(AR_1) \dots (27)$$

The same procedure can be applied to the maximum values. This quantitative comparison makes it possible to determine whether changes in quantum-dot geometry are associated with systematic changes in the magnitude and spatial localization of the hydrostatic and biaxial strain fields.

3. Results and Discussion

3.1 Three-Dimensional Hydrostatic Strain Distribution

The reconstructed hydrostatic strain field is first analyzed throughout the three-dimensional computational domain. Unlike a qualitative interpretation based solely on the color scale, the strain distribution is characterized using its minimum and maximum values, the corresponding spatial locations, and the variation ,of the field along selected profiles

The hydrostatic strain is calculated according to

$$\varepsilon_H(x,y,z) - \varepsilon_{xz}(x,y,z) + \varepsilon_{yy}(x,y,z) + \varepsilon_{zz}(x,y,z) \dots (28)$$

The minimum and maximum values within the computational domain are obtained from

$$\varepsilon_{H,\min} = \min_{(x,y,z)\in\Omega} \varepsilon_H(x,y,z) \dots (29)$$

and

$$\varepsilon_{H,\max} - \max_{(x,y,z)\in\Omega} \varepsilon_H(x,y,z) \dots (30)$$

where Ω denotes the complete computational domain The corresponding locations of the minimum and maximum values are given by

$$\mathbf{r}_{H,\min} - \arg\min_{\mathbf{r}\in\Omega} \varepsilon_H(\mathbf{r}) \dots (31)$$

and

$$\mathbf{r}_{H,\max} - \arg\max_{\mathbf{r}\in\Omega} \varepsilon_H(\mathbf{r}) \dots (32)$$

These quantities provide a direct numerical description of the spatial distribution shown in Figure 2.

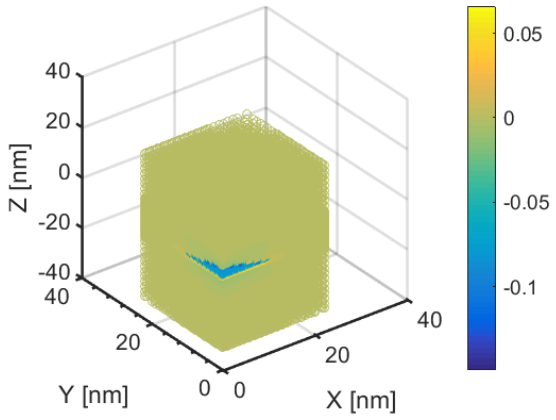


Figure 2: Three-dimensional distribution of hydrostatic strain ε_H in the pyramidal InAs/GaAs quantum dot over the selected computational domain.

For the reconstructed pyramidal InAs/GaAs quantum dot, the hydrostatic strain field exhibits a predominantly compressive character within the strained InAs region, while the surrounding GaAs matrix accommodates the elastic deformation generated by the lattice mismatch. The strain magnitude decreases spatially away from the region of strongest deformation, demonstrating the localized nature of the elastic, perturbation associated with the quantum dot [6]. The three-dimensional distribution should therefore be interpreted in terms of the calculated strain values rather than solely according to the color representation. In particular, the location and magnitude of the minimum hydrostatic strain provide a more reproducible indicator of the region experiencing the strongest volumetric compression.

Figure 2 presents the three-dimensional hydrostatic strain distribution. The corresponding numerical values of $\varepsilon_{H,\min}$, $\varepsilon_{H,\max}$, and their spatial locations should be reported directly from the reconstructed data

3.2 Biaxial Strain Distribution The biaxial strain field is analyzed separately because it describes the anisotropic component of the normal deformation and therefore provides information that is not contained in the hydrostatic component alone

The calculated biaxial strain field is given by

$$\varepsilon_B(x,y,z) - \varepsilon_{xx}(x,y,z) + \varepsilon_{yy}(x,y,z) - 2\varepsilon_{zz}(x,y,z) \dots (33)$$

Its minimum and maximum values are determined from

$$\varepsilon_{B,\min} - \min_{(x,y,z)\in\Omega} \varepsilon_B(x,y,z) \dots (34)$$

and

$$\varepsilon_{B,\max} - \max_{(x,y,z)\in\Omega} \varepsilon_B(x,y,z) \dots (35)$$

with corresponding positions

$$\mathbf{r}_{B,\min} - \arg\min_{\mathbf{r}\in\Omega} \varepsilon_B(\mathbf{r}) \dots (36)$$

and

$$\mathbf{r}_{B,\max} = \arg\max_{\mathbf{r}\in\Omega} \varepsilon_B(\mathbf{r}) \dots (37)$$

The reconstructed biaxial field exhibits a stronger spatial dependence near the quantum-dot/matrix transition than would be expected from a purely uniform deformation. This behavior reflects the difference, between the in-plane and growth-direction components of the local strain tensor Figure 3 presents the three-dimensional distribution of ε_B. The regions of negative and positive biaxial strain should be identified from the numerical values rather than from color alone.

The minimum value represents the location of the strongest negative biaxial component, whereas the maximum value identifies the strongest positive component within the computational domain. Because biaxial strain is associated with anisotropic deformation, its spatial distribution is expected to be particularly sensitive to the geometry of the pyramidal quantum dot and to the transition between the InAs inclusion and the surrounding GaAs matrix.

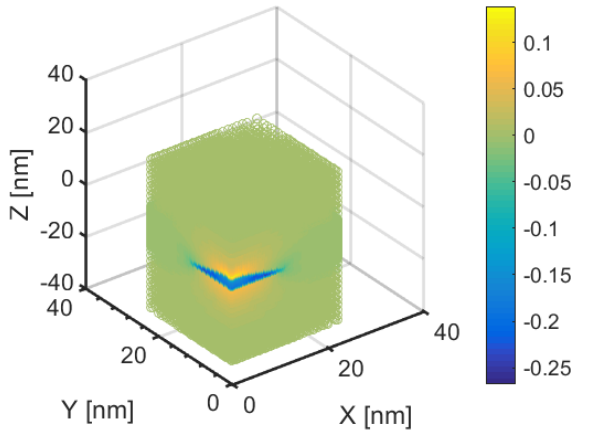


Figure 3: Three-dimensional distribution of biaxial strain εB in the pyramidal InAs/GaAs quantum.

3.3 Centerline Strain Profiles

To complement the three-dimensional maps, the strain fields are evaluated along the central vertical axis of the quantum dot. The centerline is defined by

$$x - 0, y - 0 \ldots (38)$$

and the corresponding hydrostatic and biaxial profiles are

$$\varepsilon_H^c(z) - \varepsilon_H(0,0,z) \ldots (39)$$

and

$$\varepsilon_B^c(z) - \varepsilon_B(0,0,z) \ldots (40)$$

These profiles allow the strain variation to be examined continuously along the growth direction The centerline representation is particularly useful because it removes ambiguity associated with the three-dimensional color maps and allows the position of extrema and the rate of spatial relaxation to be determined directly The distance required for the strain to approach the surrounding matrix value can be characterized by the centerline profiles. If a reference strain value ε_{ref} is defined for the unperturbed matrix, the deviation from this reference can be written as

$$\delta\varepsilon(z) - \varepsilon^c(z) - \varepsilon_{\text{ref}} \ldots (41)$$

$\varepsilon, \varepsilon_B^c$ where ε^c can represent either ε_H^c or

3.4 Strain Behavior Across the InAs/GaAs Interface

The interface region is of particular importance because the lattice mismatch is accommodated through, elastic deformation between the InAs quantum dot and the GaAs matrix

For a profile crossing the interface, the strain can be expressed as a function of the distance s along the: selected trajectory

$$\varepsilon_H(s) - \varepsilon_H\big(\mathbf{r}(s)\big) \ldots (42)$$

and

$$\varepsilon_B(s) - \varepsilon_B\big(\mathbf{r}(s)\big) \ldots (43)$$

The spatial strain variation across the interface can then be quantified by

$$\Delta\varepsilon_H - \varepsilon_{H,\text{InA s}} - \varepsilon_{H,\text{ GaAs}} \ldots (44)$$

and

$$\Delta\varepsilon_B - \varepsilon_{B,\text{In As}} - \varepsilon_{B,\text{GaAs}} \ldots (45)$$

where the values are evaluated at defined positions on the respective sides of the interface.

The interface analysis provides a quantitative description of the transition from the strongly perturbed quantum-dot region to the less perturbed surrounding matrix. This approach is preferable to describing the interface only as a "blue-to-yellow" transition because it directly relates the physical interpretation to numerical strain values.

Figure 5 represents a cross-sectional view of the same three-dimensional biaxial strain field presented in Figure 3 and does not represent an independent computational simulation.

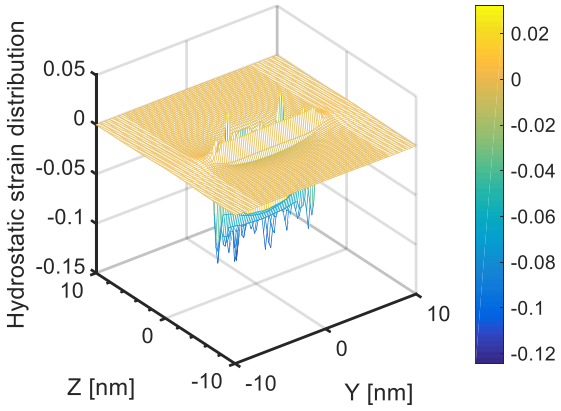


Figure 4: Cross-sectional distribution of hydrostatic strain in the y-z plane through the center of the pyramidal InAs/GaAs quantum dot.

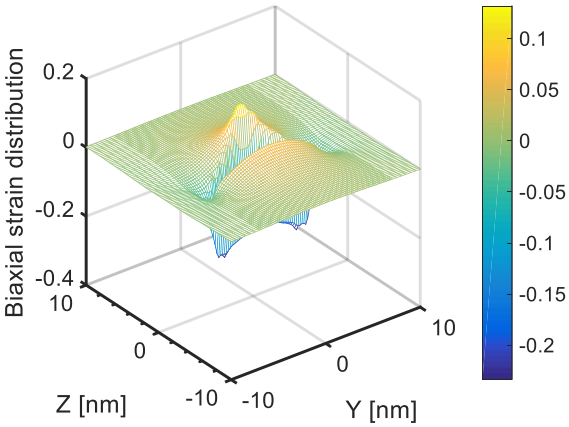


Figure 5: Cross-sectional distribution of biaxial strain in the y-z plane through the center of the pyramidal InAs/GaAs quantum dot.

3.5 Comparison of Hydrostatic and Biaxial Components

The two strain components describe different aspects of the same deformation field. Hydrostatic strain represents the volumetric component, whereas biaxial strain represents the anisotropic difference between the in-plane and growth-direction deformation [19].

Their relative magnitude at a given position can be expressed as

$$R_c(\mathbf{r}) - \frac{|\varepsilon_B(\mathbf{r})|}{|\varepsilon_H(\mathbf{r})|} \ldots (46)$$

where R_c provides a local measure of the relative contribution of the biaxial component compared with the hydrostatic component. This ratio should only be evaluated at locations where $|\varepsilon_H|$ is sufficiently different from zero to avoid numerical instability

3.5.1 Quantitative Comparison Between Hydrostatic and Biaxial Strain

The hydrostatic and biaxial strain components represent complementary aspects of the same strain tensor. Hydrostatic strain describes the volumetric component of deformation, whereas biaxial strain characterizes the directional difference between the in-plane and growth-direction components. Consequently, the two .quantities are not expected to exhibit identical spatial distributions or identical extrema

The comparison is therefore based on the following quantitative descriptors: (i) the minimum hydrostatic strain, (ii) the maximum hydrostatic strain, (iii) the minimum biaxial strain, (iv) the maximum biaxial strain, (v) the spatial coordinates of the corresponding extrema, (vi) centerline strain profiles, (vii) strain behavior across .the InAs/GaAs interface, and (viii) spatial relaxation away from the quantum dot

This quantitative approach provides a more reproducible basis for comparing the two strain components .than visual interpretation of the color maps alone [39].

Table 2. Minimum and maximum values of the reconstructed hydrostatic and biaxial strain fields and their corresponding spatial locations.

Maximum location	Maximum strain	Minimum location	Minimum strain	Strain component
nm(x_{max} , y_{max} , z_{max})	$\varepsilon_{H,max}$	nm(x_{min} , y_{min} , z_{min})	$\varepsilon_{H,\,min}$	ε_H,Hydrostatic
nm(x_{max} , y_{max} , z_{max})	$\varepsilon_{B,\,max}$	nm(x_{min} , y_{min} , z_{min})	$\varepsilon_{B,\,min}$	ε_B,Biaxial

The values reported in Table 2 are obtained directly from the reconstructed strain fields for the selected quantum-dot geometry. The extrema are reported together with their spatial coordinates to identify the regions of maximum compressive and tensile deformation. This representation enables the hydrostatic and biaxial components to be compared quantitatively while preserving their distinct physical definitions

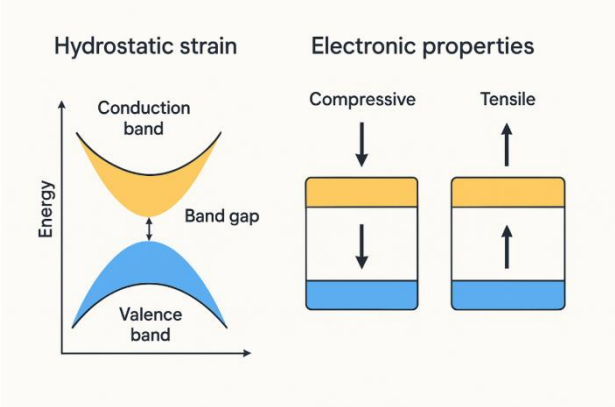


Figure 6. Hydrostatic and biaxial strain profiles along the selected spatial direction, showing the variation of strain from the quantum-dot region across the InAs/GaAs interface and into the surrounding GaAs matrix.

3.6 Aspect-Ratio Dependence

The geometry of the pyramidal quantum dot plays an important role in determining the spatial distribution of strain. In the present computational framework, the geometry is characterized by the aspect ratio [6].

$$AR = \frac{B}{H} \ldots (47)$$

where B is the square-base dimension and H is the quantum-dot height

The available strain-library solutions correspond to discrete aspect-ratio values. Changes in the aspect ratio modify the relative lateral and vertical dimensions of the pyramidal quantum dot and consequently affect the spatial distribution of both hydrostatic and biaxial strain. Therefore, the strain extrema and their corresponding spatial coordinates should be reported together with the aspect ratio used for each calculation

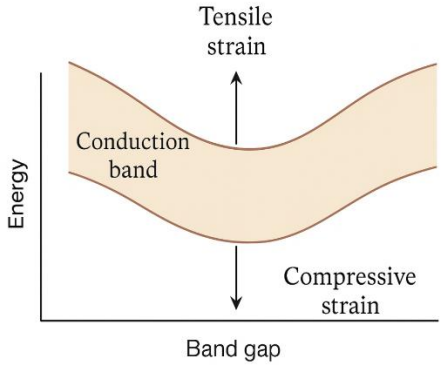


Figure 7. Dependence of the reconstructed hydrostatic and biaxial strain distributions on the aspect ratio of .the pyramidal InAs/GaAs quantum dot.

3.7 Summary of the Strain Characteristics

The reconstructed results demonstrate that the mechanical state of the pyramidal InAs/GaAs quantum dot can be described in complimentary ways by hydrostatic and biaxial strain. While the biaxial component describes the directional difference between the in-plane and growth-direction strain components, the hydrostatic component shows the volumetric contribution to the local deformation. Both strain components show spatially non-uniform distributions and gradually relax into the surrounding GaAs matrix from the quantum-dot area. The pyramidal geometry, the InAs/GaAs interface, the quantum-dot aspect ratio, and the lattice misfit between InAs and GaAs control their amplitude and spatial localization. The mechanical strain field can be more consistently described by quantitative characterisation using strain extrema and their spatial coordinates, centerline profiles, interface behavior, and spatial relaxation than by qualitative interpretation of color maps alone [40]. This investigation is limited to the mechanical strain field that has been recreated. Electronic band structures, carrier wave

functions, optical transition energies, emission spectra, carrier transport, and device performance are not directly calculated by it. Therefore, based only on the computed strain distributions, no quantitative conclusions are made about band-gap modification, carrier confinement, charge transfer, or optical-emission enhancement. Rather, the hydrostatic and biaxial strain fields that have been recreated offer a mechanically sound foundation for deformation-potential, multiband k·p, or atomistic electronic-structure calculations.

Acknowledgments
For their contributions to the computational strain framework and MATLAB-based tools utilized for the reconstruction and analysis of quantum-dot strain distributions, the authors thank Tarek Ameen and Hesam Ilatikhameneh. The current work analyzes pyramidal InAs/GaAs quantum-dot structures using the strain-library data and related computational procedures that are currently accessible. The analysis, interpretation, presentation, and findings presented in this work are the authors' responsibility.

Research Contribution
This work's primary contribution is the methodical three-dimensional reconstruction and quantitative characterisation of biaxial and hydrostatic strain fields in a pyramidal InAs/GaAs quantum dot using an aspect-ratio-dependent strain representation. In addition to identifying the spatial extrema of both strain components and analyzing their behavior across the InAs/GaAs interface and spatial relaxation within the surrounding GaAs matrix, the study consistently offers three-dimensional and central-plane representations of the strain field.
Rather than introducing a new fundamental elasticity solution, this study demonstrates the application of an aspect-ratio-dependent strain representation for the consistent and computationally efficient analysis of the three-dimensional mechanical state of a pyramidal InAs/GaAs quantum dot. The resulting strain fields establish a quantitative mechanical foundation for subsequent deformation-potential and electronic-structure calculations.

4. Conclusion
A three-dimensional computational analysis of hydrostatic and biaxial strain in a pyramidal InAs/GaAs quantum dot was presented using an aspect-ratio-dependent MATLAB reconstruction approach. The reconstructed fields reveal a spatially non-uniform strain distribution, characterized by predominantly compressive hydrostatic strain within the quantum-dot region and progressive relaxation into the surrounding GaAs matrix[6,12]. The biaxial strain exhibits a more heterogeneous spatial distribution, reflecting the directional difference between in-plane and growth-direction deformation[38,40].
The strain fields were quantitatively characterized using their minimum and maximum values, corresponding spatial coordinates, centerline profiles, interface behavior, and spatial relaxation. The results further demonstrate that the magnitude and spatial localization of the reconstructed strain fields are influenced by the InAs/GaAs lattice mismatch and the geometrical characteristics of the quantum dot, particularly its aspect ratio[40].
The present study is limited to the reconstruction and quantitative characterization of the mechanical strain field. It does not directly calculate electronic band structures, carrier wave functions, optical transition energies, carrier transport, or device performance. Therefore, no direct quantitative conclusions regarding band-gap modification, carrier confinement, or optical-emission enhancement are drawn solely from the reconstructed strain fields. Instead, the hydrostatic and biaxial strain distributions provide a quantitative mechanical input for subsequent deformation-potential, multiband $k \cdot p$, or atomistic electronic-structure calculations[12].
All things considered, this work provides a reliable three-dimensional framework for the quantitative assessment of biaxial and hydrostatic strain in pyramidal InAs/GaAs quantum dots. It offers a repeatable foundation for investigating strain-dependent electrical and optoelectronic properties as well as the impact of quantum-dot geometry and lattice mismatch on the local mechanical strain field.

References

[1] Moison, J. M., Houzay, F., Barthe, F., Leprince, L., André, E., & Vatel, O. (1994). Self-organized growth of regular nanometer-scale InAs dots on GaAs. Applied Physics Letters, 64(2), 196–198. https://doi.org/10.1063/1.111502

[2] Oglah, M. H. (2024). Analyzing the time evolution of a particle by decomposes the initial state confinement in 1D well into the lowest eigenstates energy. J. Res. Appl. Sci. Biotechnol, 3(2), 103-107. DOI: 10.55544/jrasb.3.2.17

[3] Oglah, M. H., Hasan, A. A., & Mahmood, W. I. (2025, February). Quantum confinement Bohr radius effects of quantum dots using Brus mathematical model. In AIP Conference Proceedings (Vol. 3162, No. 1, p. 020007). AIP Publishing LLC. DOI: 10.1063/5.0241782

[4] Xie, Q., Madhukar, A., Chen, P., & Kobayashi, N. P. (1995). Vertically self-organized InAs quantum box islands on GaAs(100). Physical Review Letters, 75(13), 2542–2545. https://doi.org/10.1103/PhysRevLett.75.2542

[5] Adachi, S. (2005). Properties of semiconductor alloys: Group-IV, III-V and II-VI semiconductors. Wiley.

[6] Grundmann, M., Stier, O., & Bimberg, D. (1995). InAs/GaAs pyramidal quantum dots: Strain distribution, optical phonons, and electronic structure. Physical Review B, 52(16), 11969–11981. https://doi.org/10.1103/PhysRevB.52.11969

[7] Cusack, M. A., Briddon, P. R., & Jaros, M. (1996). Electronic structure of InAs/GaAs self-assembled quantum dots. Physical Review B, 54(4), R2300–R2303. https://doi.org/10.1103/PhysRevB.54.R2300

[8] Tersoff, J., Teichert, C., & Lagally, M. G. (1996). Self-organization in growth of quantum dot superlattices. Physical Review Letters, 76(10), 1675–1678. https://doi.org/10.1103/PhysRevLett.76.1675

[9] Exploring the implementation of GaAsBi alloys as strain-reducing layers in InAs/GaAs quantum dots. (2024). Nanomaterials, 14(4), 375. https://doi.org/10.3390/nano14040375

[10] Mustafa Y Ali and Mubarak Hamad Oglah. Numerical analysis of uniaxial strain-induced modifications of the band structure and optical properties of zinc toluidine semiconductor, Int. J. Mech. Therm. Eng., 2026; 7(1): Part B, 99-108. DOI: https://www.doi.org/10.22271/27078043.2026.v7.i1b.118

[11] Cherkashin, N., Reboh, S., Hÿtch, M. J., Claverie, A., Preobrazhenskii, V. V., Putyato, M. A., Semyagin, B. R., & Chaldyshev, V. V. (2013). Determination of stress, strain, and elemental distribution within In(Ga)As quantum dots embedded in GaAs using advanced transmission electron microscopy. Applied Physics Letters, 102(17), 173115. https://doi.org/10.1063/1.4804380

[12] Vullum, P. E., Nord, M., Vatanparast, M., Thomassen, S. F., Boothroyd, C., Holmestad, R., Fimland, B.-O., & Reenaas, T. W. (2017). Quantitative strain analysis of InAs/GaAs quantum dot materials. Scientific Reports, 7, 45376. https://doi.org/10.1038/srep45376

[13] Mittelstädt, A., Schliwa, A., & Klenovský, P. (2022). Modeling electronic and optical properties of III–V quantum dots—Selected recent developments. Light: Science & Applications, 11, 17. https://doi.org/10.1038/s41377-021-00700-9

[14] Nenashev, A. V., & Dvurechenskii, A. V. (2010). Strain distribution in quantum dot of arbitrary polyhedral shape: Analytical solution. Journal of Applied Physics, 107(6), 064322. https://doi.org/10.1063/1.3357302

[15] Kosarev, A. N., Chaldyshev, V. V., & Cherkashin, N. (2022). Experimentally-verified modeling of InGaAs quantum dots. Nanomaterials, 12(12), 1967. https://doi.org/10.3390/nano12121967

[16] Park, Y. J., Kim, K. M., Park, Y. M., & Kim, E. K. (2001). Precise control of strain field for the selective formation of self-assembled InAs/GaAs quantum dots. Current Applied Physics, 1(2–3), 187–190. https://doi.org/10.1016/S1567-1739(01)00014-1

[17] Downes, J. R., Faux, D. A., & O'Reilly, E. P. (1997). A simple method for calculating strain distributions in quantum dot structures. Journal of Applied Physics, 81(10), 6700–6702. https://doi.org/10.1063/1.365210

[18] Pryor, C. (1998). Eight-band calculations of strained InAs/GaAs quantum dots compared with one-, four-, and six-band approximations. Physical Review B, 57(12), 7190–7195. https://doi.org/10.1103/PhysRevB.57.7190

[19] Stier, O., Grundmann, M., & Bimberg, D. (1999). Electronic and optical properties of strained quantum dots modeled by 8-band (k\cdot p) theory. Physical Review B, 59(8), 5688–5701. https://doi.org/10.1103/PhysRevB.59.5688

[20] Andreev, A. D., Downes, J. R., Faux, D. A., & O'Reilly, E. P. (1999). Strain distributions in quantum dots of arbitrary shape. Journal of Applied Physics, 86(1), 297–305. https://doi.org/10.1063/1.370728

[21] Shchukin, V. A., & Bimberg, D. (1999). Spontaneous ordering of nanostructures on crystal surfaces. Reviews of Modern Physics, 71(4), 1125–1171. https://doi.org/10.1103/RevModPhys.71.1125

[22] Barker, J. A., & O'Reilly, E. P. (2000). Theoretical analysis of electron-hole alignment in InAs-GaAs quantum dots. Physical Review B, 61(20), 13840–13851. https://doi.org/10.1103/PhysRevB.61.13840

[23] Pusep, Y. A., Zanelatto, G., da Silva, S. W., Galzerani, J. C., et al. (1998). Raman study of interface modes subjected to strain in InAs/GaAs self-assembled quantum dots. Physical Review B, 58(4), R1770–R1773. https://doi.org/10.1103/PhysRevB.58.R1770

[24] Bir, G. L., & Pikus, G. E. (1974). Symmetry and strain-induced effects in semiconductors. Wiley.

[25] Pearson, G. S., & Faux, D. A. (2000). Analytical solutions for strain in pyramidal quantum dots. Journal of Applied Physics, 88(2), 730–736. https://doi.org/10.1063/1.373729

[26] Kegel, I., Metzger, T. H., Lorke, A., Peisl, J., Stangl, J., Bauer, G., García, J. M., & Petroff, P. M. (2000). Nanometer-scale resolution of strain and interdiffusion in self-assembled InAs/GaAs quantum dots. Physical Review Letters, 85(8), 1694–1697. https://doi.org/10.1103/PhysRevLett.85.1694

[27] Liu, X., Luo, Z., Zhou, X., Wei, J., Wang, Y., Guo, X., Lang, Q., & Ding, Z. (2019). Theoretical study of stress and strain distribution in coupled pyramidal InAs quantum dots embedded in GaAs by finite element method. The European Physical Journal B, 92, 138. https://doi.org/10.1140/epjb/e2019-100090-5

[28] Adhikary, S., Halder, N., Chakrabarti, S., Majumdar, S., Ray, S. K., Herrera, M., Bonds, M., & Browning, N. D. (2010). Investigation of strain in self-assembled multilayer InAs/GaAs quantum dot heterostructures. Journal of Crystal Growth, 312(5), 724–729. https://doi.org/10.1016/j.jcrysgro.2009.11.067

[29] Zieliński, M. (2012). Including strain in atomistic tight-binding Hamiltonians: An application to self-assembled InAs/GaAs and InAs/InP quantum dots. Physical Review B, 86(11), 115424. https://doi.org/10.1103/PhysRevB.86.115424

[30]Califano, M., & Harrison, P. (2002). Composition, volume, and aspect ratio dependence of the strain distribution, band lineups and electron effective masses in self-assembled pyramidal $In_{1-x}Ga_xAs$/GaAs and Si_xGe_{1-x}/Si quantum dots. Journal of Applied Physics, 91(1), 389–398. https://doi.org/10.1063/1.1410318

[31] Selen, L. J. M., van IJzendoorn, L. J., de Voigt, M. J. A., & Koenraad, P. M. (2000). Evidence for strain in and around InAs quantum dots in GaAs from ion-channeling experiments. Physical Review B, 61(12), 8270–8275.https://doi.org/10.1103/PhysRevB.61.8270

[32] Califano, M., & Harrison, P. (2000). Presentation and experimental validation of a single-band, constant-potential model for self-assembled InAs/GaAs quantum dots. Physical Review B, 61(16), 10959–10965. DOI: https://doi.org/10.1103/PhysRevB.61.10959

[33]Pearson, G. S., & Faux, D. A. (2000). Analytical solutions for strain in pyramidal quantum dots. Journal of Applied Physics, 88(2), 730-736. https://doi.org/10.1063/1.373729

[34] Zhang, X., & Sharma, P. (2005). Size dependency of strain in arbitrary shaped anisotropic embedded quantum dots due to nonlocal dispersive effects. Physical Review B, 72(19), 195345. https://doi.org/10.1103/PhysRevB.72.195345

[35] Jaskólski, W., Zieliński, M., Bryant, G. W., & Aizpurua, J. (2006). Strain effects on the electronic structure of strongly coupled self-assembled InAs/GaAs quantum dots: Tight-binding approach. Physical Review B, 74(19), 195339. https://doi.org/10.1103/PhysRevB.74.195339

[36]Kuo, M. K., Lin, T. R., Hong, K. B., Liao, B. T., Lee, H. T., & Yu, C. H. (2006). Two-step strain analysis of self-assembled InAs/GaAs quantum dots. Semiconductor Science and Technology, 21(5), 626–632. https://doi.org/10.1088/0268-1242/21/5/010

[37] Ngo, C. Y., Yoon, S. F., Fan, W. J., & Chua, S. J. (2006). Effects of size and shape on electronic states of quantum dots. Physical Review B, 74(24), 245331. https://doi.org/10.1103/PhysRevB.74.245331

[38] Yang, X. F., Chen, X. S., Lu, W., & Fu, Y. (2008). Effects of shape and strain distribution of quantum dots on optical transition in the quantum dot infrared photodetectors. Nanoscale research letters, 3(12), 534. DOI 10.1007/s11671-008-9175-8

[39] Bimberg, D., Grundmann, M., & Ledentsov, N. N. (1998). Quantum dot heterostructures. Wiley. No DOI located; ISBN 978-0-471-97388-1. Stangl, J., Holý, V., & Bauer, G. (2004). Structural properties of self-organized semiconductor nanostructures. Reviews of Modern Physics, 76(3), 725–783. https://doi.org/10.1103/RevModPhys.76.725

[40] Ilatikhameneh, H., Ameen, T. A., Klimeck, G., & Rahman, R. (2016). Universal behavior of atomistic strain in self-assembled quantum dots. IEEE Journal of Quantum Electronics, 52(7), 1–8. https://doi.org/10.1109/JQE.2016.2573959